Finite Difference Calculations of Unsteady Premixed Flame-Flow Interactions

S. R. Mulpuru* and G. B. Wilkin*
Atomic Energy of Canada Limited, Pinawa, Manitoba, Canada

A conservative, explicit, hybrid, finite difference method based on the techniques of flux splitting and flux correction is presented for the calculation of one-dimensional, premixed flame-flow interactions. The intent has been to eliminate flame structure resolution, which is computationally expensive, and focus on the pressures and temperatures resulting from the interactions. Accordingly, the flame is treated as a discontinuity propagating in a Eulerian grid and obeying a specified, empirical burning law. Comparisons with closed-form solutions of flame-flow interaction problems involving shock, expansion wave, and contact discontinuity show that the method correctly predicts the outcome of the interactions.

Nomenclature

a = local sound speed
A = duct cross-sectional area
$[A]$ = Jacobian matrix
B = surface area enclosing a volume
c = dimensionless constant
e = total energy density
f = eigenvector
$\boldsymbol{F}$ = flux vector
G = momentum density
$\hat{n}$ = unit normal vector pointing outward from a surface
p = pressure
q = energy of reaction at 0 K per unit mixture mass
$\boldsymbol{Q}$ = vector of mass, momentum, and energy densities
S = burning velocity
t = time
U = flow velocity
V = nodal volume
W = velocity of the boundary, or flame velocity
x = position coordinate
Δx = space step
Δt = time step
β = positive parameter
ϵ = specific internal energy
γ = ratio of specific heats
λ = eigenvalue
ρ = mass density

Subscripts

b = burnt gas
F = flame
L,R = interfaces in Fig. 2a
u = unburnt gas

Superscripts

$( )^*$ = energy of formation included
$( )^+$ = unburnt side adjacent to the flame
$( )^-$ = burnt side adjacent to the flame

Presented as Paper 83-1917 at the AIAA Sixth Computational Fluid Dynamics Conference, Danvers, Mass., July 13-15, 1983; received Aug. 2, 1983; revision received April 9, 1984.

*Research Staff, Systems Analysis Branch.

I. Introduction

ANALYSIS of unsteady combustion, which occurs for example in internal combustion engines or accidental fuel-air explosions, requires the capability of predicting the resulting flowfield and overpressure and temperature transients. The processes relevant for the analysis are ignition, laminar and/or turbulent flame propagation, and interactions among the flame, flow, and system boundary which result in a complicated flow pattern consisting of shock and expansion waves and contact discontinuities. Deflagration to detonation transition (DDT), with its concomitant large overpressures, can occur as a result of these interactions.[1]

We are concerned here with finite difference solutions of premixed flame-flow interactions. The governing equations[2] are the conservation equations of mass, momentum, and energy of a chemically reactive flow, together with equations defining submodels for chemical kinetics and turbulence. Numerical solution of these equations within the flame zone, where the hydrodynamic and chemical processes are intimately coupled, poses some difficulties. Earlier work on this subject includes that of Oran et al.,[3] Boni et al.,[4] and Dwyer and Sanders.[5] Two difficulties reported in these references are the excessive computation time required to solve the detailed kinetic models, and the interference of either spurious oscillations or numerical diffusion with the reaction rates and physical diffusion within the flame zone. The reasons behind these difficulties are as follows.

First, the time scales of the chemical and hydrodynamic phenomena are different by several orders of magnitude. Using time steps small enough to finely resolve fast chemical kinetic processes involving several species and reactions is computationally expensive. Second, properties vary rapidly within the flame zone. In a Eulerian system, higher order (≥ 2) approximations of the convective terms of the conservation equations generate spurious oscillations in the vicinity of large gradients.[6] These oscillations may trigger convergence to physically false solutions.[7] They can be suppressed either by using first-order accurate solutions which implicitly contain numerical diffusion or by explicitly adding the diffusion to the higher order solutions. To ensure that numerical diffusion does not swamp physical diffusion, it is necessary to maintain the cell Reynolds number $Re_c = U(\Delta x)/\nu$ [the ratio of the numerical diffusivity ($U\Delta x$) to the physical diffusivity (ν)] much less than unity. This can be accomplished by reducing the grid size Δx within the flame zone, which in turn necessitates reducing the time step size to satisfy the Courant stability limit (in the explicit methods). This translates again into higher computation cost. Using a Gedanken numerical experiment on simple one-dimensional

flame propagation in a 1-m-long tube, Oran and Boris[8] recently showed that it is prohibitively expensive to finely resolve the chemical and hydrodynamic processes. It is therefore necessary to introduce appropriate empiricism into the problem in order to reduce the computation cost.

The burning velocity of a premixed flame quantifies the aggregate effect of the interaction of the hydrodynamic and chemical kinetic phenomena within the flame zone. It is defined as the flame front velocity normal to and relative to the unburnt gas velocity. Experimentally measured and correlated empirical relations are available in the literature[9-13] for both laminar and turbulent burning velocities as functions of the unburnt mixture thermodynamic state and flow properties. The empirical relations can be used to specify the flame burning velocity in models that embed a discontinuous, propagating flame in a computational grid. The discontinuous flame model eliminates calculation of the flame structure and yet has the potential to yield reliable flowfield information. The subject of this paper is the construction of such a model for one-dimensional flow, and demonstration of the calculation of flame-flow interactions.

Besides the flame, the flowfield involves other sharp propagating gradients (waves). Between the two types of what are known as "shock capturing" and "shock fitting" methods, we chose a method of the former type to calculate the flowfield. Kurylo et al.[14] used a method of the latter type to analyze flowfields generated by accelerating flames. While the fitting methods yield more accurate results, they are difficult to implement because they require "remembering" when and where the waves arise, tracking them in position and time, and explicitly handling each of the various possible interactions among the waves. The shock capturing methods, in contrast, calculate the waves and their interactions automatically whenever and wherever they occur and are easier to implement. To reduce computation cost, we chose a shock capturing method recently developed by one of the authors,[15] based on the techniques of flux splitting[16] and flux correction.[17-20]

We describe in Sec. II the embedding of a discontinuous flame in a Eulerian grid, briefly review in Sec. III the method to calculate the flowfield, and in Sec. IV we compare the finite difference and closed-form solutions of some flame-flow interaction problems.

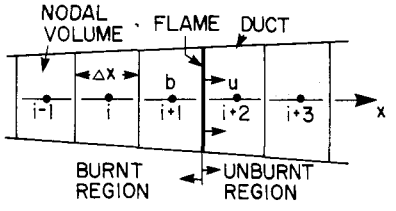

Fig. 1 Discretization of the duct into nodal volumes. Flame is defined as a (moving) boundary between two volumes.

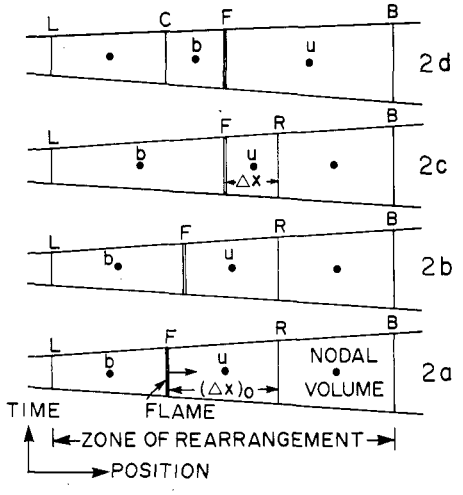

Fig. 2 Grid rearrangement when the nodal volume ahead of flame shrinks to a preset value.

II. Flame Embedding in a Eulerian Grid

Grid Arrangement

A duct of variable cross-sectional area is chosen to illustrate the grid arrangement for a moving flame (Fig. 1). This arrangement and the equations to be derived later are also applicable to cylindrical and spherical geometries.

The duct is discretized into a number of contiguous nodal volumes (Fig. 1), at the center of which volume-averaged mass, momentum, and energy densities are defined. The flame is defined initially to be the interface of two adjacent volumes separating the burnt and unburnt regions. The flame is advanced in position and time, subject to satisfying a specified empirical relation for burning velocity and the conservation of mass, momentum and energy.

As the flame advances (Figs. 2a and b), the volume behind it (b) grows while the one ahead of it (u) shrinks. To avoid numerical difficulties, it is necessary to rearrange the grid in the neighborhood of the flame before the shrinking volume assumes too small a value. When Δx (Fig. 2c) of the shrinking volume is less than a specified fraction ($\frac{1}{2}$) of its initial volume $(\Delta x)_0$, the interface R ahead of it is eliminated and the two nodes adjacent to the eliminated interface are replaced by one node between the flame F and the interface B (Fig. 2d). The mass, momentum, and energy densities at the new node are defined as volume-weighted averages of the values in the eliminated nodes. This results in numerical mixing (diffusion), which can be reduced by using a finer grid, but cannot be eliminated entirely. The enlarged volume behind the flame (Fig. 2c) is split into two (Fig. 2d) by inserting an interface (C) at the location where the flame interface was initially situated (Fig. 2a), thus recovering the original volume. The procedure is repeated when the Δx of the new volume ahead of the flame, bounded by interfaces F and B (Fig. 2d) shrinks again to the preset value. Note that the flame always remains as an interface between two volumes, and the number of nodal volumes, both within the rearranged zone and globally, remains the same. Therefore, modification of information in the computer memory corresponding to the grid rearrangement is required only in the immediate vicinity of the flame zone, and hence is efficient.

Equations for Volumes with Moving Boundary

The discretized nodal volumes (Fig. 1) are of two types. In the first type, the flame is part of the boundary enclosing the volume, which is allowed to change as the flame moves. In the second type, the boundary is stationary. For volumes of the first type, it is convenient to write the governing mass, momentum, and energy conservation equations in integral form. These equations of an ideal, compressible flow of a perfect gas mixture, for a volume V whose bounding surface B moves with an arbitrary velocity W are[21]:

$$\frac{\mathrm{d}}{\mathrm{d}t}\int_V \rho \mathrm{d}V + \int_B \rho(U-W)\cdot\hat{n}\mathrm{d}B = 0 \tag{1}$$

$$\frac{\mathrm{d}}{\mathrm{d}t}\int_V G\mathrm{d}V + \int_B G(U-W)\cdot\hat{n}\mathrm{d}B + \int_B \hat{n}p\mathrm{d}B = 0 \tag{2}$$

$$\frac{\mathrm{d}}{\mathrm{d}t}\int_V e^*\mathrm{d}V + \int_B [e^*(U-W)+pU]\cdot\hat{n}\mathrm{d}B = 0 \tag{3}$$

where

$$G=\rho U \tag{4}$$

$$e^*=e+\rho\epsilon_0 \tag{5}$$

$$e=\rho(\epsilon+U^2/2) \tag{6}$$

$$p=(\gamma-1)\rho\epsilon \tag{7}$$

The energy equation (3) is written in terms of e^* (which includes the energy of formation ϵ_0) in order to account for the energy transfer due to burning between two nodal volumes (b and u in Fig. 1). For all the nodal volumes where no burning takes place, this equation can be rewritten in terms of e by virtue of Eq. (1) as:

$$\frac{\mathrm{d}}{\mathrm{d}t}\int_V e\,\mathrm{d}V+\int_B [e(U-W)+pU]\cdot\hat{n}\,\mathrm{d}B=0 \tag{8}$$

After simplifying for the one-dimensional case, Eqs. (1-3) can be written for the two volumes b and u (Fig. 2a) adjacent to the flame as:

$$\frac{\mathrm{d}(\boldsymbol{Q}^*V)_b}{\mathrm{d}t}=(\boldsymbol{AF}^*)_L-(\boldsymbol{AF}^*)_F^{+}+\boldsymbol{R}_b \tag{9}$$

$$\frac{\mathrm{d}(\boldsymbol{Q}^*V)_u}{\mathrm{d}t}=(\boldsymbol{AF}^*)_F^{-}-(\boldsymbol{AF}^*)_R+\boldsymbol{R}_u \tag{10}$$

Here, the subscripts denote either a node or an interface. The vectors $\boldsymbol{Q}^*$, $\boldsymbol{F}^*$, and $\boldsymbol{R}$ are given in terms of averaged quantities as:

$$\boldsymbol{Q}^*=\begin{bmatrix}\rho\\ G\\ e^*\end{bmatrix};\quad \boldsymbol{F}^*=\begin{bmatrix}G\\ G^2/\rho+p\\ G/\rho(e^*+p)\end{bmatrix};\quad \boldsymbol{R}=\begin{bmatrix}0\\ p(A_R-A_L)\\ 0\end{bmatrix} \tag{11}$$

$(\boldsymbol{F}_F^*)^+$ and $(\boldsymbol{F}_F^*)^-$ denote fluxes on the unburnt and burnt sides, respectively, of the flame. Assuming that the properties just behind the flame are the same as those at the nearest node of the same side, and using the definition of the burning velocity,

$$S=W-(G/\rho)_u \tag{12}$$

the fluxes can be written as:

$$(\boldsymbol{F}^*)^+=\begin{bmatrix}-\rho_u S\\ -G_u S+P_u\\ -e_u^* S+(pG/\rho)_u\end{bmatrix} \tag{13}$$

$$(\boldsymbol{F}^*)^-=\begin{bmatrix}-\rho_b[S+(G/\rho)_u-(G/\rho)_b]\\ -G_b[S+(G/\rho)_u-(G/\rho)_b]+p_b\\ -e_b^*[S+(G/\rho)_u-(G/\rho)_b]+p_b(G/\rho)_b\end{bmatrix} \tag{14}$$

Equations (9) and (10) are also applicable to cylindrical and spherical geometries. In these cases, the cross-sectional area A assumes a linear and quadratic relationship, respectively, with the spatial coordinate.

The conservation of mass, momentum, and energy flux across the flame discontinuity dictates satisfying the Rankine-Hugoniot relations

$$(\boldsymbol{F}_F^*)^-=(\boldsymbol{F}_F^*)^+ \tag{15}$$

Numerical Solution

The time rates of change of properties in the two nodes adjacent to the flame are described by Eqs. (9) and (10). We advance the numerical solution of these equations from time t to $t+\Delta t$ in two fractional steps. For this purpose, the terms on the right-hand sides of these equations are split into two groups. Convection fluxes through the stationary interfaces L and R [$(\boldsymbol{AF}^*)_L$ and $(\boldsymbol{AF}^*)_R$] comprise the first group. The terms belonging to the second group, $(\boldsymbol{AF}^*)_F^{\pm}$, $(\boldsymbol{AF}^*)_{\bar{F}}$, and $\boldsymbol{R}_u$, $\boldsymbol{R}_b$ account for the fluxes due to flame movement and momentum source terms.

The first fractional step involves calculating provisional values of the dependent variables by advancing convection through the stationary interfaces, while freezing the flame movement:

$$(\boldsymbol{Q}^*V)_b^{\overline{t+\Delta t}}=(\boldsymbol{Q}^*V)_b^t+\Delta t\cdot(\boldsymbol{AF}^*)_L^t \tag{16}$$

$$(\boldsymbol{Q}^*V)_u^{\overline{t+\Delta t}}=(\boldsymbol{Q}^*V)_u^t-\Delta t\cdot(\boldsymbol{AF}^*)_R^t \tag{17}$$

Here, the superscript $\overline{t+\Delta t}$ indicates a provisional value.

The second fractional step corrects the provisional values by accounting for the flame movement in the time interval Δt:

$$(\boldsymbol{Q}^*V)_b^{t+\Delta t}=(\boldsymbol{Q}^*V)_b^{\overline{t+\Delta t}}-\Delta t\cdot[(\boldsymbol{AF}^*)_F^{\pm}]^a+\Delta t\cdot[(\boldsymbol{R})_b^t+(\boldsymbol{R})_b^{t+\Delta t}]/2 \tag{18}$$

$$(\boldsymbol{Q}^*V)_u^{t+\Delta t}=(\boldsymbol{Q}^*V)_u^{\overline{t+\Delta t}}+\Delta t\cdot[(\boldsymbol{AF}^*)_{\bar{F}}]^a+\Delta t\cdot[(\boldsymbol{R})_u^t+(\boldsymbol{R})_u^{t+\Delta t}]/2 \tag{19}$$

Here the superscript a denotes an average value in the time interval Δt. The volumes at the advanced time $t+\Delta t$ can be expressed by integrating the flame velocity W [Eq. (12)] using the trapezoidal rule as:

$$V_b^{t+\Delta t}=V_b^t+\Delta t[\{A_F(S+(G/\rho)_u)\}^{t+\Delta t}+\{A_F(S+(G/\rho)_u)\}^t]/2 \tag{20}$$

and by volume conservation,

$$V_b^{t+\Delta t}+V_u^{t+\Delta t}=V_b^t+V_u^t \tag{21}$$

Since the conservation of mass, momentum, and energy dictates that the average flame flux terms in Eqs. (18) and (19) be equal, addition of these equations results in cancellation of these terms, yielding:

$$(\boldsymbol{Q}^*V)_b^{t+\Delta t}+(\boldsymbol{Q}^*V)_u^{t+\Delta t}=(\boldsymbol{Q}^*V)_b^{\overline{t+\Delta t}}+(\boldsymbol{Q}^*V)_u^{\overline{t+\Delta t}}+\Delta t\cdot[(\boldsymbol{R}_b^t+\boldsymbol{R}_b^{t+\Delta t})+(\boldsymbol{R}_u^t+\boldsymbol{R}_u^{t+\Delta t})]/2 \tag{22}$$

Equation (22) is a set of conservation statements for the combined nodal volumes b and u (Fig. 1). It eliminates the need to define explicitly the average flame fluxes in Eqs. (18) and (19), and provides instead three equations for the simultaneous solution of the six unknowns $(\boldsymbol{Q}_b^*)^{t+\Delta t}$ and $(\boldsymbol{Q}_u^*)^{t+\Delta t}$ in the two nodes adjacent to the flame. The other three equations are provided by the Rankine-Hugoniot relations [Eq. (15)] at the advanced time $t+\Delta t$:

$$[(\boldsymbol{F}_F^*)^-]^{t+\Delta t}=[(\boldsymbol{F}_F^*)^+]^{t+\Delta t} \tag{23}$$

Before solving iteratively, we rewrite Eqs. (22) and (23) in terms of the total energy e instead of e^* (splitting the energy of formation) by substituting Eq. (5) and using the first component (mass) equation of each of Eqs. (22) and (23) as:

$$(\boldsymbol{QV})_b^{t+\Delta t}+(\boldsymbol{QV})_u^{t+\Delta t}=(\boldsymbol{QV})_b^{\overline{t+\Delta t}}+(\boldsymbol{QV})_u^{\overline{t+\Delta t}}+\Delta t[(\boldsymbol{R}_b^t+\boldsymbol{R}_b^{t+\Delta t})+(\boldsymbol{R}_u^t+\boldsymbol{R}_u^{t+\Delta t})]/2+\boldsymbol{H}_I \tag{24}$$

$$[(F_F)^-]^{t+\Delta t} = [(F_F)^+]^{t+\Delta t} + H_2 \tag{25}$$

where

$$H_1 = \begin{bmatrix} 0 \\ 0 \\ -[(\rho V)_u^{t+\Delta t} - (\rho V)_u^{\overline{t+\Delta t}}]q \end{bmatrix} \tag{26}$$

$$H_2 = \begin{bmatrix} 0 \\ 0 \\ \rho_u S q \end{bmatrix} \tag{27}$$

and q is the energy of reaction at 0 K per unit mixture mass, given by:

$$q = (\epsilon_0)_u - (\epsilon_0)_b \tag{28}$$

Here, Q, F, $(F_F)^+$, and $(F_F)^-$ are the counterparts of Q^*, F^*, $(F_F^*)^+$, $(F_F^*)^-$ obtained by omitting the superscript * in Eqs. (11), (13), and (14). The burning velocity S in Eqs. (20) and (27) can be expressed empirically as a function of the unburnt mixture thermodynamic state as

$$S = S(Q)_u \tag{29}$$

A specific form of relation (29) used in testing the numerical method can be found in Eq. (52).

Equations (24) and (25), together with the auxiliary relations (29), (20), and (21), constitute six nonlinear algebraic equations in six unknowns $(Q_b)^{t+\Delta t}$ and $(Q_u)^{t+\Delta t}$. These are solved iteratively using the Newton-Raphson method until specified convergence criteria are achieved.

III. Numerical Method for Volumes with Fixed Boundaries

Solution Aspects of Equations

The boundaries of all the nodal volumes (Fig. 1) in the burnt and unburnt regions, except for the two adjacent to the flame, are stationary ($W = 0$). For such a nodal volume i, Eqs. (1), (2), and (8) can be simplified to a form analogous to Eqs. (9) or (10) as:

$$\frac{\mathrm{d}(AQ)i}{\mathrm{d}t} = \{(AF)_{i-\frac{1}{2}} - (AF)_{i+\frac{1}{2}}\}/(x_{i+\frac{1}{2}} - x_{i-\frac{1}{2}}) + \begin{bmatrix} 0 \\ p_i(A_{i+\frac{1}{2}} - A_{i-\frac{1}{2}})/(x_{i+\frac{1}{2}} - x_{i-\frac{1}{2}}) \\ 0 \end{bmatrix} \tag{30}$$

In the limit of $(x_{i+\frac{1}{2}} - x_{i-\frac{1}{2}})$ tending to zero, Eq. (30) assumes the familiar weak conservation form:

$$\frac{\partial(AQ)}{\partial t} + \frac{\partial(AF)}{\partial x} = Z \tag{31}$$

where

$$Z = \begin{bmatrix} 0 \\ p\partial A/\partial x \\ 0 \end{bmatrix} \tag{32}$$

Based on the analysis of a homogeneous, linear, scalar version of Eq. (31), Godunov[6] showed that higher-order (≥ 2) finite difference schemes yield spurious oscillations in the vicinity of sharp gradients, whereas the first-order accurate schemes do not. However, higher order schemes yield more accurate results in the smooth regions. A way to exploit the desirable features of each method is to use a hybrid scheme that weights the solution of a higher order scheme as heavily as possible with that of a first-order scheme, subject to the restriction that the final weighted solution be free of spurious extrema. Zalesak[20] designed such a weighting procedure and showed that it was a generalization of the flux correction procedure developed by Boris et al.[17-19]

Equation (31) is solved using an explicit hybrid scheme that was recently developed by one of the authors[15] for the homogeneous form of Eq. (31). The scheme, briefly described below, involves estimating a lower order and a higher order accurate solution based on flux splitting,[16] and weighting the two estimates.

Split-Conservation Form

Stegar and Warming[16] showed that the flux vector F [Eq. (11) with omitted superscript *] satisfies the relation

$$F = [A]Q \tag{33}$$

where $[A]$ is the Jacobian $[\partial F/\partial Q]$, and F can be written in a split form using the properties of $[A]$ as:

$$F = \sum_{\ell=1}^{3} \lambda_\ell f_\ell \tag{34}$$

where λ_1, λ_2, and λ_3 are the distinct eigenvalues of $[A]$, and f_1, f_2, and f_3 are the eigenvectors corresponding to the eigenvalues. Using relations (33) and (34) it has been shown[15] that the vector Q is composed of the eigenvectors f_ℓ as

$$Q = \sum_{\ell=1}^{3} f_\ell \tag{35}$$

Specifically,

$$\lambda_1 = U, \quad \lambda_2 = (U+a), \quad \lambda_3 = (U-a) \tag{36}$$

$$f_1 = \frac{\rho(\gamma-1)}{2\gamma}\begin{bmatrix} 2 \\ 2U \\ U^2 \end{bmatrix}; \quad f_2 = \frac{\rho}{2\gamma}\begin{bmatrix} 1 \\ (U+a) \\ (U+a)^2/2 + w \end{bmatrix}$$

$$f_3 = \frac{\rho}{2\gamma}\begin{bmatrix} 1 \\ (U-a) \\ (U-a)^2/2 + w \end{bmatrix} \tag{37}$$

where

$$w = \frac{(3-\gamma)a^2}{2(\gamma-1)} \tag{38}$$

One can easily check relations (34) and (35) using Eqs. (36-38). By virtue of relations (34) and (35), one can see that Eq. (31) possesses a split-conservation form:

$$\frac{\partial}{\partial t}\left\{A\sum_{\ell=1}^{3} f_\ell\right\} + \frac{\partial}{\partial x}\left\{A\sum_{\ell=1}^{3} \lambda_\ell f_\ell\right\} = Z \tag{39}$$

Numerical Method

Equation (35) suggests that the solution increment $\delta(AQ)$ over a time step Δt can be built up linearly on a finite difference grid by summing the corresponding increments of the

Table 1 Properties obtained by closed-form solutions (see Figs. 3-5)

Region	Problem 1			Problem 2			Problem 3		
	ρ, kg/m^3	u, m/s	a, m/s	ρ, kg/m^3	u, m/s	a, m/s	ρ, kg/m^3	u, m/s	a, m/s
1	0.8671	6.762	409.6	1.587	283.2	469.5	0.1859	−61.96	803.8
2	0.1878	−0.02525	804.1	0.4289	194.8	817.2	0.3809	555.1	860.6
3	0.1901	−10.10	805.0	0.5440	−2.169	834.2	0.5082	302.5	882.5
4	0.1904	−10.10	804.3	0.5603	−2.169	822.0	0.5823	302.5	824.4
5	0.8769	−11.33	410.5	1.936	93.24	489.4	1.948	400.5	499.1
6	N/A	N/A	N/A	2.128	139.9	498.8	0.8672	6.762	409.6

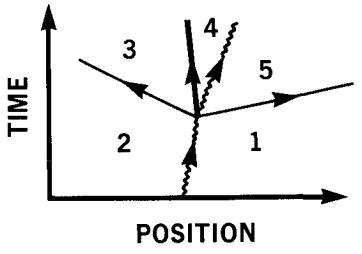

Fig. 3 Wave system resulting from a step increase in flame speed. Interfaces of adjacent regions denote waves. These are: 1-2, initial flame; 4-5, flame with increased speed; 2-3 and 5-1, shock waves resulting from step increase in flame speed; 3-4, contact discontinuity. Properties of each region are given in Table 1.

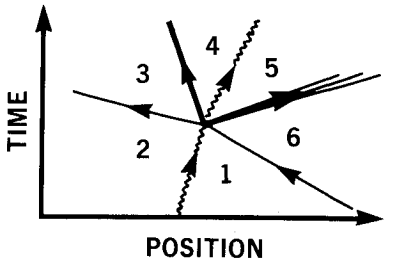

Fig. 4 Wave system resulting from a shock-flame head-on collision. Interface 1-2 denotes the flame before the collision; 4-5, flame after collision; 1-6, incident shock; 2-3, transmitted shock; 5-6, reflected expansion wave; and 3-4, contact discontinuity.

eigenvectors:

$$\delta_i(AQ)=\delta_i\left(A\sum_{\ell=1}^{3}f_\ell\right) \tag{40}$$

where

$$\delta_i\phi=\phi_i^{n+1}-\phi_i^n \tag{41}$$

and ϕ_i^n denotes $\phi(x_0+i\Delta x,\ t_0+n\Delta t)$. To facilitate calculation of the individual increments on the right-hand side of Eq. (40), Eq. (39) can be further split into individual vector continuity equations:

$$\frac{\partial}{\partial t}(Af_\ell)+\frac{\partial}{\partial x}\{A(\lambda_\ell f_\ell)\}=\boldsymbol{K}_\ell;\quad \ell=1,2,3 \tag{42}$$

where $\boldsymbol{K}_\ell$ satisfies the relation:

$$\sum_{\ell=1}^{3}\boldsymbol{K}_\ell=\boldsymbol{Z} \tag{43}$$

One-step, explicit, conservative schemes for the solution of Eq. (42) that use three-point, central-difference operators can be written in a general form:

$$\delta_i(Af_\ell)=\{(\boldsymbol{C}-\boldsymbol{D})_\ell\}_{i-\frac{1}{2}}-\{(\boldsymbol{C}-\boldsymbol{D})_\ell\}_{i+\frac{1}{2}}+\boldsymbol{K}_\ell\Delta t;\quad \ell=1,2,3 \tag{44}$$

where $\boldsymbol{C}$ and $\boldsymbol{D}$ represent the fluxes that are due to convection and numerical diffusion, respectively. They are defined, incorporating both a first-order accurate upwind scheme and a second-order scheme, as follows[15]:

$$(\boldsymbol{C}_\ell)_{i+\frac{1}{2}}=\frac{1}{2}\frac{\Delta t}{\Delta x}\{A(\lambda f)_\ell\}_{i+1}^n+\{A(\lambda f)_\ell\}_i^n;\quad \ell=1,2,3 \tag{45}$$

$$(\boldsymbol{D}_\ell)_{i+\frac{1}{2}}=\frac{1}{2}\frac{\Delta t}{\Delta x}\{(\lambda_\ell)_{i+\frac{1}{2}}^n\}b_{i+\frac{1}{2}}[\{A(\lambda f)_\ell\}_{i+1}^n-\{A(\lambda f)_\ell\}_i^n];\quad \ell=1,2,3 \tag{46}$$

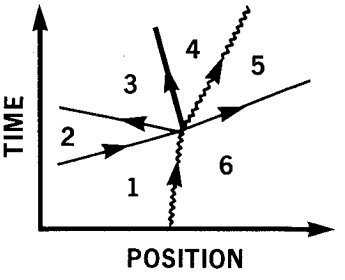

Fig. 5 Wave system resulting from a shock-flame merging. Interface 6-1 denotes initial flame; 2-1, shock before merging; 2-3, reflected shock; 5-6, transmitted shock; 4-5, flame after the encounter; and 3-4, contact discontinuity.

where

$$(\lambda_\ell)_{i+\frac{1}{2}}^n=\{(\lambda_\ell)_{i+1}^n+(\lambda_\ell)_i^n\}/2;\quad \ell=1,2,3 \tag{47}$$

and $(\beta_\ell)_{i+\frac{1}{2}}$ is a dimensionless positive parameter. The larger the value of $(\beta_\ell)_{i+\frac{1}{2}}$, the more numerical diffusion the scheme has. The choice:

$$(\beta_\ell)_{i+\frac{1}{2}}=1;\quad \ell=1,2,3 \tag{48}$$

defines a first-order accurate upwind scheme, and

$$(\beta_\ell)_{i+\frac{1}{2}}=|(\lambda_\ell)_{i+\frac{1}{2}}|\Delta t/\Delta x;\quad \ell=1,2,3 \tag{49}$$

defines a scheme similar to the second-order Lax-Wendroff scheme. Substituting Eq. (44) into Eq. (40), one obtains the following for the advancement of the solution vector (AQ):

$$\delta_i(AQ)=\sum_{\ell=1}^{3}[\{\boldsymbol{C}-\boldsymbol{D})_\ell\}_{i-\frac{1}{2}}-\{(\boldsymbol{C}-\boldsymbol{D})_\ell\}_{i+\frac{1}{2}}]+\boldsymbol{Z}\cdot\Delta t \tag{50}$$

Equations (50) and (45-48) define a first-order upwind scheme. The same equations, with Eq. (48) replaced by Eq. (49), define a second-order scheme similar to the Lax-Wendroff scheme. For both schemes, the stability condition,

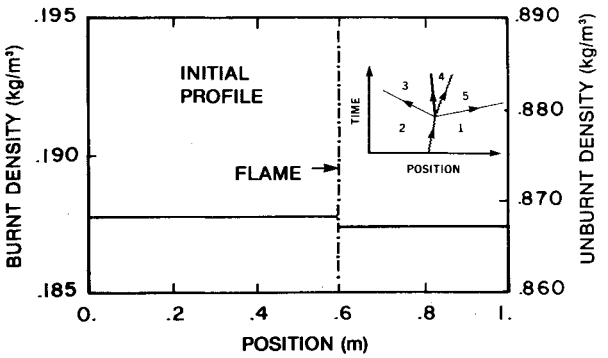

Fig. 6a Initial density profile for the first problem (step increase in flame speed).

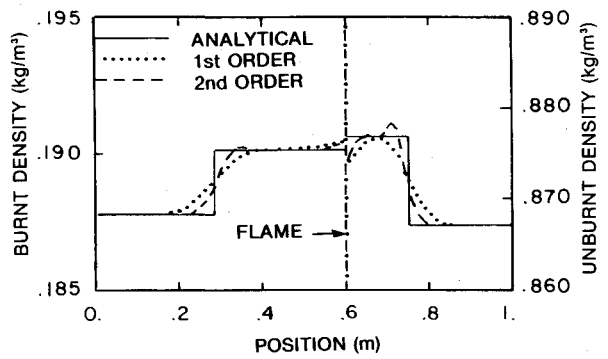

Fig. 6b First- and second-order accurate solutions (dashed lines) at an instant after step increase in flame speed. Solid line indicates analytical solution. The four step changes in the solid line profile starting from the left indicate shock wave, contact discontinuity, flame, and shock wave, respectively (see Fig. 3). The dashed vertical line indicates flame location separating burnt and unburnt regions.

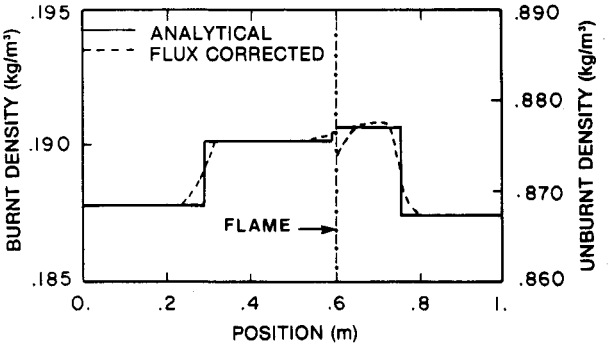

Fig. 6c Flux-corrected solution at the same instant as in Fig. 6b.

based on a linear (constant λ_ℓ), homogeneous version of Eq. (42), is:

$$|\lambda_\ell|\,\Delta t/\Delta x \leq 1; \quad \ell = 1,2,3 \tag{51}$$

Delegating the source (last) term $Z\Delta t$ in Eq. (50) to a fractional step, the lower and higher order solutions are weighted by using, without change, the procedure developed by Zalesak.[20] The resulting hybrid scheme, in conjunction with that outlined in Sec. II for the solution at the two special nodes adjacent to the flame, is used here to calculate the flame-flow iteractions.

IV. Flame-Flow Interactions

It is well known that flames subjected to perturbations generate pressure waves.[22-25] The interactions among these waves, the flame, and the system boundary result in a

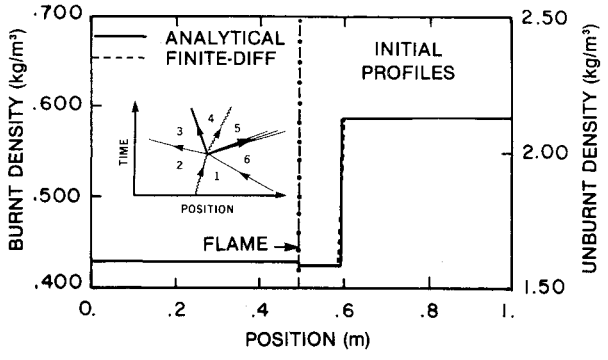

Fig. 7a Initial density profiles for the problem of shock-flame head-on collision.

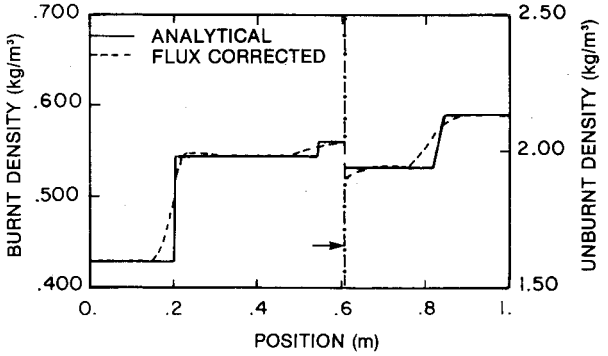

Fig. 7b Flux-corrected solution obtained by weighting the first- and second-order accurate solutions.

complicated flow pattern consisting of shocks, expansion waves, and contact discontinuities. In this section, the finite difference solutions are benchmarked on some of these interactions. The geometry considered is a duct of uniform cross-sectional area. In particular, the following three problems are presented: a) step increase in the flame speed; 2) shock-flame head-on collision; and 3) shock-flame merging.

The wave systems resulting from these interactions are shown in Figs. 3-5; a description is given in the captions. Each of these interactions leads to the formation of new regions 3, 4, and 5. It is of interest to calculate the uniform properties in the new regions. Oppenheim et al.[26] developed the vector polar method—a graphical technique to calculate such wave interaction processes. Here, we eschew the inconvenience of a graphical technique and instead solve numerically closed-form algebraic relations that define these properties in the new regions. Using the two conditions that the pressures and velocities on both sides of the contact discontinuity (Figs. 3-5) must be equal, one can express the properties in the new regions in closed form by two nonlinear algebraic equations in two independent variables; these being the strengths (pressure ratios) of the two waves bounding the new regions 3, 4, and 5. We solved the two equations iteratively by the Newton-Raphson method until specified convergence criteria were achieved. Since the equations are complicated, we found it expedient to evaluate the Jacobian required in these calculations numerically. The closed-form solutions thus obtained are compared with the finite difference solutions in Figs. 6-8. The properties of each region as determined by the closed-form solution are presented in Table 1 for all three problems.

Problem Setup

Stoichiometric hydrogen-air was the unburnt mixture chosen. Based on the work of Heimel[9] and Drell and Belles,[10] an empirical relation for the burning velocity of this mixture

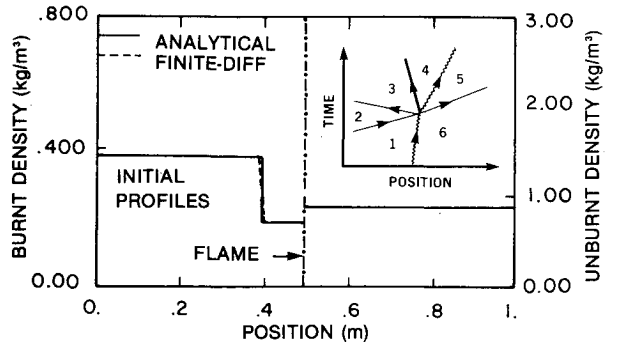

Fig. 8a Initial density profiles for the shock-flame merging problem.

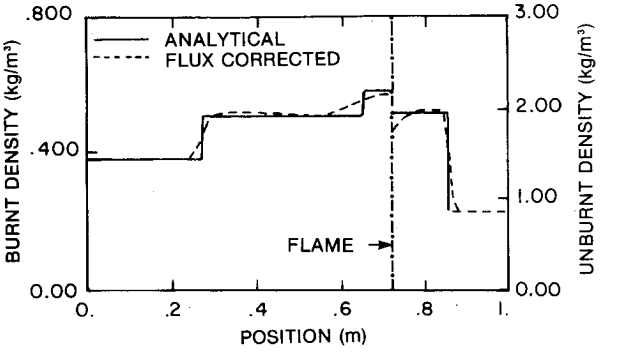

Fig. 8b Flux-corrected solution obtained by weighting the first- and second-order accurate solutions.

$$S = c \cdot S_0 (p/p_0)^{0.1} (T/T_0)^{1.721} \tag{52}$$

was chosen to demonstrate the flame-flow calculations. Here, the subscript *0* denotes reference values: $T_0 = 298$ K, $p_0 = 101$ kPa (1 atm), and $S_0 = 1.85$ m/s; the laminar burning velocity at the reference conditions. c is an arbitrary dimensionless constant which is assigned a value of 1 in the first problem and 10 in the second and third problems. The ratio of specific heats for the burnt mixture was specified to be 1.17—the equilibrium value for constant-pressure combustion. A 1-m long duct of uniform cross section was discretized into 100 nodes. For each problem, initial conditions at the nodes were defined to correspond to the wave system. The jumps in the properties across the waves were specified to occur between two adjacent nodes. Since the focus is on wave interactions, the waves were positioned initially such that the boundaries are far enough away to be "unaware" of the interaction in the time period considered. Consequently, the boundary conditions were enforced to be time-invariant initial conditions. The time step was determined at each solution time based on a Courant number of 0.5.

Finite Difference Solutions

The solutions for the first problem are presented in Figs. 6a-d. The density profile of the initial flame is shown in Fig. 6a. The flame location is indicated by the dashed vertical line separating the unburnt and burnt regions. Since the densities in the two regions differ greatly (about an order of magnitude), we have used for clarity different ordinate scales for the two regions.

The density profiles predicted by the different versions of the solution are presented in Figs. 6b and c; all are for the same elapsed time after the step increase in the initial flame speed. In the first-order accurate solution (Fig. 6b), the sharp gradients are smeared excessively, but no oscillations appear. The second-order solution yields sharper profiles but generates spurious postshock oscillations. The flux-corrected solution (Fig. 6c) obtained by a nonlinear weighting of the lower and higher order solutions alleviates the oscillations while reducing the smearing somewhat. The smearing of the sharp gradients in Eulerian grids is inevitable because, however small a quantity of mass, momentum, or energy crosses the boundaries of a nodal volume, it gets mixed over the entire volume in the process of defining an averaged quantity at the center of the volume. The flux-correction procedure reduces the smearing effect, but cannot eliminate it.

The initial density profiles for the shock-flame collision (second) problem are shown in Fig. 7a. The flux-corrected solutions at an instant after the collision are compared with the analytical solution in Fig. 7b. The outcome of the interactions, including property jumps across the shock and expansion waves and wave speeds, are predicted correctly, but the smearing problem persists. Similar results are obtained for the problem of shock-flame merging (Figs. 8a and 8b).

V. Conclusions

A procedure to embed a discontinuous flame in a Eulerian grid and propagate the flame according to a specified empirical burning law has been presented. A merit of this approach is that it eliminates costly flame structure calculations and focuses on the pressure and temperature information. A conservative, explicit, finite difference method incorporating the flame embedding procedure has been benchmarked on flame-flow interaction problems. The method is based on flux splitting, which lends itself to efficient estimation of first- and second-order accurate solutions and thereby to a weighting of these two in a flux correction procedure. The first-order scheme yields no spurious oscillations, but diffuses the sharp gradients excessively. The second-order scheme produces sharper profiles, but generates erroneous postshock oscillations. The flux-corrected solution alleviates the undesirable features of the two. The result is correct prediction of the outcome of the interactions, including wave speed and property jumps across the waves. However, the smearing of the sharp gradients persists. The extent of smearing can be limited by using a finer grid in regions where large gradients exist. This aspect and extension of the method to two spatial dimensions will be the subjects of future work.

References

[1] Lee, J.H.S. and Moen, I. O., "The Mechanism of Transition from Deflagration to Detonation in Vapour Cloud Explosions," *Progress in Energy and Combustion Science*, Vol. 6, 1980, pp. 359-389.

[2] Williams, F. A., *Combustion Theory: The Fundamental Theory of Chemically Reacting Flow Systems*, 1st ed., Addison-Wesley, Mass., 1965, pp. 1-17.

[3] Oran, E. S., Boris, J. P., Young, T. P., Flanigan, M., Burks, T., and Picone, M., "Numerical Simulations of Detonations in Hydrogen-Air and Methane-Air Mixtures," *Eighteenth Symposium (International) on Combustion*, The Combustion Institute, 1981, pp. 1641-1649.

[4] Boni, A. A., Wilson, C. W., Chapman, M., and Cook, J. L., "A Study of Detonation in Methane/Air Clouds," *Acta Astronautica*, Vol. 5, 1978, pp. 1153-1169.

[5] Dwyer, H. A. and Sanders, B. R., "Modeling of Unsteady Combustion Phenomena," AIAA Paper 77-136, Jan. 1977.

[6] Godunov, S. K., "Finite Difference Method for Numerical Computation of Discontinuous Solutions of the Equations of Fluid Dynamics," *Mathematicheskii Sbornik*, Vol. 47 (89), No. 3, 1959, pp. 271-306; also, Cornell Aeronautical Lab. Translation.

[7] Harten, A., Hyman, J. M., and Lax, P. D., "On Finite-Difference Approximations and Entropy Conditions for Shocks," *Communications on Pure and Applied Mathematics*, Vol. 39, 1976, pp. 297-322.

[8] Oran, E. S. and Boris, J. P., "Detailed Modeling of Combustion Systems," *Progress in Energy and Combustion Science*, Vol. 7, 1981, pp. 1-72.

[9]Heimel, S., "Effect of Initial Mixture-Temperature on Burning Velocity of Hydrogen—Air Mixtures with Preheating and Simulated Preburning," NACA TN-4156, Oct. 1957.

[10]Drell, I. L. and Belles, F. E., "Survey of Hydrogen Combustion Properties," NACA-TR-1383, 1958.

[11]Andrews, C. E., Bradley, D., and Lwakabamba, S. B., "Turbulence and Turbulent Flame Propagation—A Critical Appraisal," *Combustion and Flame*, Vol. 24, 1975, pp. 285-304.

[12]Rallis, C. J. and Garforth, A. M., "The Determination of Laminar Burning Velocity," *Progress in Energy and Combustion Science*, Vol. 6, 1980, pp. 303-329.

[13]Liu, D.D.S. and MacFarlane, R. F., "Laminar Burning Velocity of Hydrogen-Air and Hydrogen-Air-Steam Flames," *Combustion and Flame*, Vol. 49, 1983, pp. 59-71.

[14]Kurylo, J., Dwyer, H. A., and Oppenheim, A. K., "Numerical Analysis of Flowfields Generated by Accelerating Flames," *AIAA Journal*, Vol. 18, March 1980, pp. 302-308.

[15]Mulpuru, S. R., "A Finite-Difference Solution Scheme for the Inviscid Compressible-Flow Equations Based on Flux Vector Splitting and Flux Correction," *Mathematics and Computers in Simulation*, Vol. 25, No. 4, 1983, pp. 309-320.

[16]Stegar, J. L. and Warming, R. F., "Flux Vector Splitting of the Inviscid Gasdynamic Equations with Application to Finite Difference Methods," NASA-TM-78605, July 1979.

[17]Boris, J. P. and Book, D. L., "Flux-Corrected Transport. 1. SHASTA, A Fluid Transport Algorithm that Works," *Journal of Computational Physics*, Vol. 11, 1973, pp. 38-69.

[18]Book, D. L., Boris, J. P., and Hain, K., "Flux-Corrected Transport II: Generations of the Method," *Journal of Computational Physics*, Vol. 18, No. 3, 1975, pp. 248-283.

[19]Boris, J. P. and Book, D. L., "Flux-Corrected Transport III. Minimal-Error FCT Algorithms," *Journal of Computational Physics*, Vol. 20, No. 4, 1976, pp. 397-431.

[20]Zalesak, S. K., "Fully Multidimensional Flux-Corrected Transport Algorithms for Fluids," *Journal of Computational Physics*, Vol. 31, 1979, pp. 335-362.

[21]Thompson, P. A., *Compressible-Fluid Dynamics*, 1st ed., McGraw-Hill Book Co., Inc., New York, 1972, pp. 39-42.

[22]Chu, B. T., "On the Generation of Pressure Waves at a Plane Flame Front," *Fourth Symposium (International) on Combustion*, Williams & Wilkins, Baltimore, Md., 1953, pp. 603-612.

[23]Laderman, A. J. and Oppenheim, A. K., "Initial Flame Acceleration in an Explosive Gas," *Proceedings of the Royal Society of London*, Vol. A268, 1962, pp. 153-180.

[24]Kuhl, A. L., Kamel, M. M., and Oppenheim, A. K., "On Flame Generated Self-Similar Blast Waves," *Fourteenth Symposium (International) on Combustion*, The Combustion Institute, 1973, pp. 1201-1214.

[25]Guirao, C. M., Bach, G. G., and Lee, J. H., "Pressure Waves Generated by Spherical Flames," *Combustion and Flame*, Vol. 27, 1976, pp. 341-351.

[26]Oppenheim, A. K., Urtiew, P. A., and Ladermann, A. J., "Vector Polar Method for the Evaluation of Wave Interaction Processes," *Archiwum Budowy Maszyn* [Archives of Mechanical Engineering], Vol. 11, No. 3, 1964, pp. 441-495.